

Tunneling blockade and single-photon emission in GaAs double quantum wells

M. Yuan,^{1,*} A. Hernández-Mínguez,¹ K. Biermann,¹ and P. V. Santos¹

¹*Paul-Drude-Institut für Festkörperelektronik, Leibniz-Institut im
Forschungsverbund Berlin e. V., Hausvogteiplatz 5-7, 10117 Berlin, Germany*
(Dated: March 12, 2022)

We report on the selective excitation of single impurity-bound exciton states in a GaAs double quantum well (DQW). The structure consists of two quantum wells (QWs) coupled by a thin tunnel barrier. The DQW is subject to a transverse electric field to create spatially indirect inter-QW excitons with electrons and holes located in different QWs. We show that the presence of intra-QW charged excitons (trions) blocks carrier tunneling across the barrier to form indirect excitons, thus opening a gap in their emission spectrum. This behavior is attributed to the low binding energy of the trions. Within the tunneling blockade regime, emission becomes dominated by processes involving excitons bound to single shallow impurities, which behave as two-level centers activated by resonant tunneling. The quantum nature of the emission is confirmed by the anti-bunched photon emission statistics. The narrow distribution of emission energies (~ 10 meV) and the electrical connection to the QWs make these single-exciton centers interesting candidates for applications in single-photon sources.

The interplay between resonant tunneling and inter-particle interactions in low-dimensional quantum systems gives rise to interesting phenomena in the transport of single particles. A prototype example is the Coulomb blockade, where repulsive Coulomb interaction blocks the transport through a localized state between two reservoirs. [1, 2] This blockade, which expresses itself as plateaus between steps in the current *versus* voltage characteristics, is a direct signature of single carrier transport.

In this paper, we report on an analogous blockade phenomenon during the transport of exciton-related species across a thin tunnel barrier between two semiconductor quantum wells (QWs) (cf. Fig. 1(a)). Each QW supports intra-QW neutral excitons (denoted here as direct excitons, DX) as well as intra-QW charged excitons (trions, T). A transverse electric field F_z applied across the double QW (DQW) structure controls the tunneling probability and enables the creation of spatially indirect, inter-QW excitons (IXs) consisting of electrons and holes resident in different QWs (cf. Fig. 1(b)). The energy of IX is tunable by F_z due to quantum-confined Stark effect (QCSE). [3, 4] We show that the low binding energy of trions blocks carrier tunneling over a range of applied fields and, thus, the formation of IX states. Unlike Coulomb blockade, which arises from the repulsive interaction between electrons, the tunneling blockade reported here originates from the attractive exciton-carrier interaction leading to trion formation. Within the blockade regime, tunneling becomes restricted to resonant processes leading to the excitation of individual excitons bound to shallow impurities. These states act as electrically controlled two levels systems: their quantum nature is evidenced by the anti-bunched photon emission statistics. The electric control and narrow distribution of emission energies make these bound-exciton emitters potential candidates for GaAs-based single-photon sources.

The studies were carried out on the (Al,Ga)As struc-

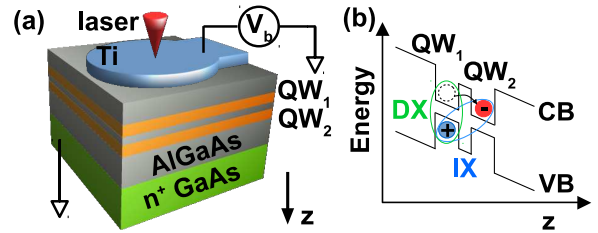


FIG. 1. (a) (Al,Ga)As DQW structure on doped GaAs (001) substrate. The DQW is embedded in the intrinsic region of a Schottky diode defined by the semitransparent Ti top contact. The bias voltage V_b is applied between the top contact and the doped substrate. The photoluminescence (PL) studies were carried out at 4.2 K by exciting carriers using a focused laser spot. (b) Energy band diagram of the DQW showing the conduction (CB) and valence bands (VB) profiles under an electric field, which leads to IX formation.

ture illustrated in Fig. 1(a). The sample was grown by molecular beam epitaxy (MBE) on n-doped GaAs(001) substrate. The DQW consists of two 16 nm-wide GaAs QWs separated by a 4 nm-thick $\text{Al}_{0.33}\text{Ga}_{0.67}\text{As}$ barrier. The DQW is subjected to an electric field F_z generated by a bias voltage V_b applied between a 10 nm-thick semitransparent top titanium contact[5–7] and the n-doped substrate.

The optical studies were carried out at 4.2 K using a microscopic photoluminescence (μ -PL) setup with spatial and spectral resolutions of 0.6 μm and 0.08 meV, respectively. Figure 2(a) displays the bias dependence of the PL intensity I_{PL} recorded by exciting the sample with a focused laser beam (diameter $\phi_L = 1.2 \mu\text{m}$) and integrating the emission over a 7.5 μm -long and 1 μm -wide slit across the Ti gate. The laser wavelength and power were $\lambda = 780$ nm (1.59 eV) and $P = 240$ nW, respectively. Further experimental details can be found in the supplementary material (SM), Sec. SM1. The PL

bias map shows the typical spectral lines from DXs, IXs, and Ts.[8, 9] The strong trion signal signals the availability of free carriers. The energy and intensity of T line remain constant over a wide range of biases denoted as FB in Fig. 2(a) (i.e., for biases V_b between 0.5 and 1.2 V compensating the built-in potential of the Schottky junction). Within this range, the flow of free carriers between the QWs screens the applied electric field across the DQW structure, thus inhibiting IX formation. The transition region between the FB and IX regimes is characterized by an enhanced DX emission together with a reduction of the trion intensity. The latter is attributed to the depletion of free carriers in one of the QWs as these carriers tunnel to and accumulate in the adjacent QW.[8, 10] Carrier accumulation in one of the QWs also accounts for the non-linear bias dependence of the IX energy close to the FB-IX transition.[8]

More interesting spectral features appear when mapping the FB-IX transition range using a much lower excitation densities, as illustrated in Fig. 2(b). Strikingly, the IX line does not smoothly “branch off” from the DX and T lines but only appears for $V_b < 0.25$ V, thus indicating that its formation is blocked within the bias range BR indicated in the figure. The latter results in a spectral gap between T energy and the onset of the IX emission given by $\Delta E_B = 5.7$ meV. Furthermore, the IX appearance at $V_b \sim 0.25$ V is accompanied by a drastic reduction of the T intensity, which indicates that the IXs result from the dissociation of T states. Finally, several sharp emission lines appear in the IX blockade regime BR. These lines can be grouped into two families (labeled as DX^b and IX^b and indicated by the dot-dashed lines in Fig. 2(b)) with bias dependence similar to the ones for free DX and IX species, respectively. The energies of the individual lines are typically between 1.5 to 10 meV lower than the T emission.

The observation of multiple sharp lines in Fig. 2(b) arises from the integration of the emission over an extended area on the sample surface. Figure 2(c) displays a similar bias map recorded by collecting the emission over a much smaller sample area (corresponding to the resolution limit of $0.4 \mu\text{m}^2$), where individual lines can be observed (labeled as D_1 and D_2). The energy distribution of such emission lines cover the typical energy range of excitons bound to shallow impurities. Natural candidates for the impurities are silicon (donor) and carbon (acceptor), which are the most common impurities present in the MBE growth. Interestingly, these lines mainly appear over the narrow bias range BR and are generally not present in the IX bias range, where their excitation should also be energetically favorable. This behavior indicates that these individual states are excited via a resonant process taking place over a narrow range of biases.

The correlation between the appearance of bound exciton and IX lines, on the one hand, and the disappearance

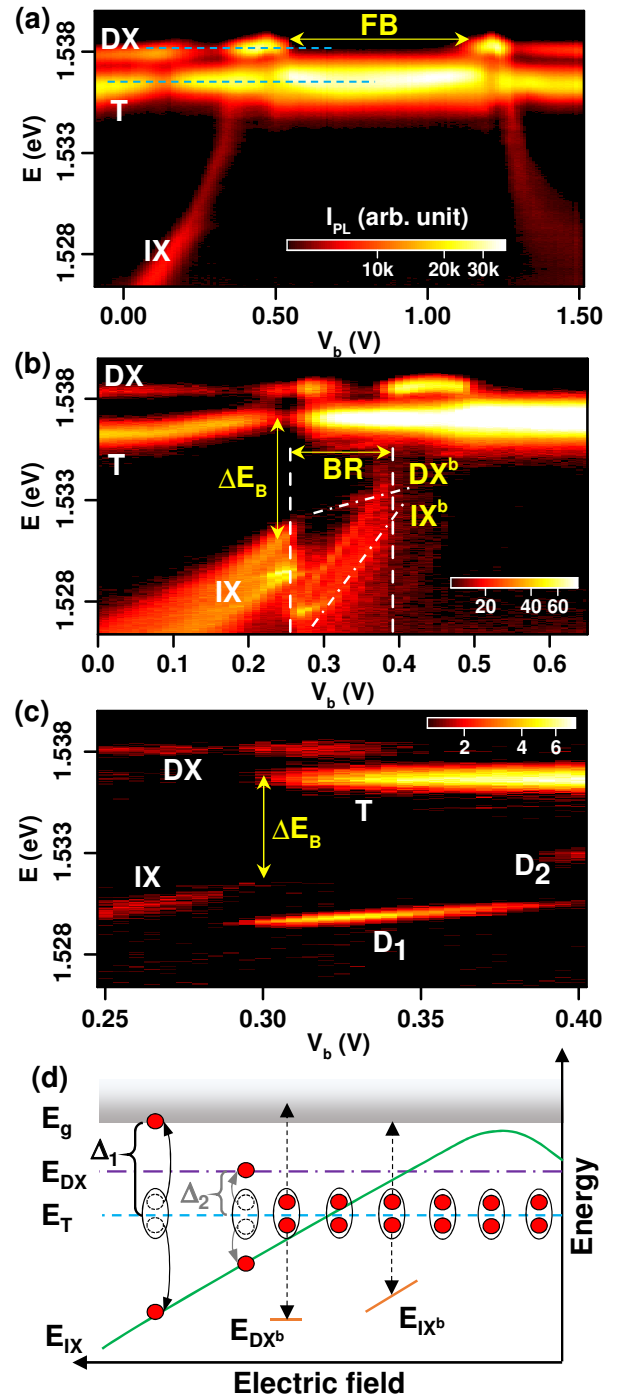


FIG. 2. (a) Spatially integrated PL vs. bias voltage V_b recorded under a high laser power ($P = 240$ nW). FB denotes the flat band region. (b) Idem, but recorded under a low power ($P = 0.6$ nW), for bias in the IX-FB transition region of (a). The formation of IX is blocked within the spectral windows indicated by ΔE_B . Individual lines DX^b and IX^b associated with excitons bound to shallow impurities appear in the blockade region BR between the FB and IX regimes. (c) Bias maps recorded with high spatial resolution showing sharp lines (D_1 and D_2) attributed to excitons bound to shallow impurities. (d) Energies of different exciton species in a DQW as a function of the electric field. The arrows show possible trion dissociation processes.

of T on the other hand, suggests that the former results from dissociation of T, governed by energy conservation. The electric field dependence of the energy E_i of the different excitonic species ($i = \text{DX}, \text{IX}, \text{T}$) is summarized in Fig. 2(c).[11] The non-monotonous electric field dependence of $E_{\text{IX}}(F_z)$ results from the combined effect of the QCSE and the electric field dependence of IX binding energy ΔE_{IX} . [12] Two trion dissociation scenarios involving resonant tunneling and IX formation can be envisaged. For simplicity, we will consider electron trions (a similar argument applies to hole trions). In the first, a trion dissociates via the emission of a free carrier in the same QW (with energy equal to the band gap energy E_g) and the tunneling of the extra electron to form an IX, as indicated by the solid curved arrows in Fig. 2(d). Energy conservation requires that

$$E_{\text{T}} - E_{\text{IX}}(F_z) \geq E_g - E_{\text{T}} = \Delta_1. \quad (1)$$

IX formation will thus be blocked within an energy range Δ_1 below the trion energy. Alternatively, the free electron of the previous process may form a DX in the presence of a free hole. In this case, the condition to lift the IX formation blockade reads:

$$E_{\text{T}} - E_{\text{IX}}(F_z) \geq E_{\text{DX}} - E_{\text{T}} = \Delta_2. \quad (2)$$

Since this process requires a an extra particle, it is expected to be suppressed at low excitation densities.

According to the calculations in Ref. 12, the binding energy of DX, $\Delta E_{\text{DX}} = E_{\text{DX}} - E_g \approx -5.7$ meV for the DQW structure used here. From Fig. 2(a), we obtain $\Delta_2 = 1.6$ meV, thus yielding $\Delta_1 = 7.3$ meV. The measured ΔE_B at different laser powers (cf. Fig. 2 and SM2) typically yield $\Delta E_B = 5 \pm 1$ meV, in reasonable agreement with Δ_1 for low excitation densities. At high excitation power and high temperature, the blockade feature cannot be identified anymore (see SM2).

The energy conservation constraint imposed by Eqs. 1 and 2 stabilizes trions and opens a gap in the emission spectrum of free IX species. Within the gap, trions can still be resonantly converted into lower energy excitons bound to an impurity, e.g. DX^b and IX^b (their energies labeled as E_{DX^b} and E_{IX^b} , respectively), indicated by the straight arrows in Fig. 2(d). We illustrate two possible mechanisms for the conversion. In the first case, the T in one QW dissociates into a free particle and a DX bound to a shallow center in the same QW (DX^b). In the second case, one of the trion particles tunnels across the barrier to form an IX^b bound to a shallow center in the adjacent QW. (Note that the free particle can also be replaced by a DX if an extra hole is available.) These two processes yield bound species with the bias dependences corresponding to the ones for the DX^b and IX^b states[13, 14] indicated by the dot-dashed lines in Fig. 2(b) (e.g., both D_1 and D_2 in Fig. 2(c) behave as DX^b).

We now concentrate on the properties of the bound exciton states. Their spatial distribution was determined

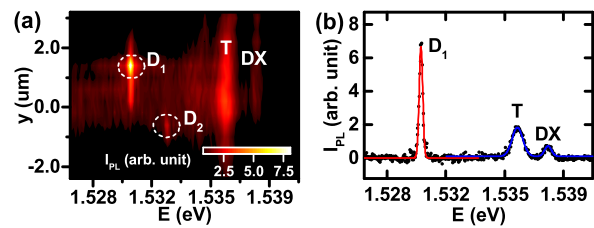


FIG. 3. (a) Spectral PL image showing the spatial distribution of free excitons (DX and T) and excitons bound to shallow centers (D_1 and D_2). The excitons were remotely excited by a focused laser spot placed at $y = 0$. The DQW is biased at the edge of the flatband. (b) PL spectrum (background subtracted) at the location of D_1 (symbols). The superimposed lines are Gaussian fits.

by spatially resolved PL maps recorded while biasing the structure in the BR, as illustrated in Fig. 3(a). The sample was excited by a focused laser spot at $y = 0$ and the emission recorded as a function of the distance from the excitation spot. In addition to the lines from DX and T, the figure shows localized peaks from two defect centers D_1 and D_2 at 1530.4 meV and 1532.7 meV, respectively (the same defects as in Fig. 2(c)), which are populated by carriers diffusing from the excitation spot. The shallow centers are typically between 2 to 4 μm apart, thus yielding an areal density $n_d \approx 10^7 \text{cm}^{-2}$. Figure 3(b) displays a cross-section of Fig. 3(a) at the position of D_1 (maximum emission) at $y = 1.4 \mu\text{m}$. The spectral line shape is fitted by a Gaussian profile (red) with a full width at half maximum of $\hbar\Gamma_S = 0.26$ meV. The latter is significantly narrower than the DX and T linewidths (of 0.42 meV and 0.66 meV, respectively, cf. blue curves). The temperature dependence of the emission intensity of the bound exciton (see SM3 for details) yields an activation energy E_A comparable to the energy red-shift with respect to T, thus indicating that the decay is caused by thermal dissociation into T. The PL intensity and linewidth, however, saturate for temperature lower than 5 K. The line width broadening at 4 K is probably due to charge fluctuation.[15]

Information about the internal structure of the bound excitons was obtained from measurements under a magnetic field B_z applied along the DQW growth axis (cf. Fig. 4(a)). The field splits the emission peak into a Zeeman doublet with energy splittings $\Delta E^{(z)}$ and average energies increasing with B_z . The B_z dependence of the doublet energy is summarized by the blue circles in Fig. 4(b) and can be expressed as:

$$E = \Delta E^{(d)} \pm \frac{1}{2} \Delta E^{(z)} = \frac{e^2}{8\mu} \langle \rho^2 \rangle B_z^2 \pm \frac{1}{2} g \mu_B B_z. \quad (3)$$

Here, e is the electron charge, μ the in-plane reduced excitonic mass satisfying $\frac{1}{\mu} = \frac{1}{m_e} + \frac{1}{m_{hh}}$, where $m_e = 0.0665 m_0$ and $m_{hh} = 0.34 m_0$ denote the in-plane electron and heavy-hole masses, respectively, and m_0 is the

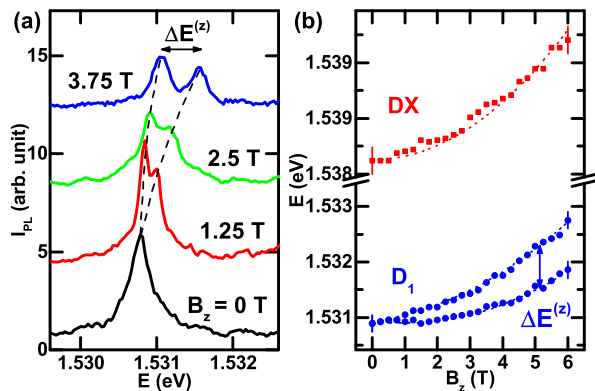


FIG. 4. (a) PL spectra of D_1 recorded under different magnetic fields B_z applied along the growth axis (the curves are shifted vertically for clarity) showing the Zeeman splitting ΔE_z as well as the diamagnetic blue-shift $\Delta E^{(d)}$. (b) Peak energies of the DX (squares) and D_1 (circles) resonances as a function of B_z . The dashed lines are fits to Eq. 3. Due to the larger linewidths, the Zeeman splitting cannot be clearly resolved for the DXs.

electron rest mass.[16] μ_B is the Bohr magneton and g the exciton Landé g -factor, which depends on the corresponding g -factors for holes and electrons.[17] The first term on the r.h.s is the diamagnetic blue-shift $\Delta E^{(d)}$ resulting from the confinement of excitonic wave function by B_z , which depends on the spatial extent of the exciton wave function ρ . [18, 19]

The blue dashed lines superimposed on the experimental points are fits to Eq. 3, which yield $g = 2.2$ and $\rho = 9$ nm. This value for the effective exciton radius is in good agreement with the one reported for excitons bound to shallow donors.[20]. Figure 4(b) also shows the magnetic field dependence of the DX resonance (red squares). Due to the large spectral linewidth, the Zeeman splitting cannot be clearly resolved. From the quadratic dependence of the diamagnetic shifts (cf. Eq. 3), we extract an exciton radius of 12 nm. In addition to the quadratic diamagnetic behavior, one also observes small discontinuities in the field dependence, probably due to Landau quantization of the free carriers.

Motivated by the narrow linewidths of the bound excitons as well as their spectral separation from free exciton states, we investigate the bound-excitons' potential as two-level systems emitting single photons. The two-level characteristic can be inferred by the saturation of emission intensity with increasing laser excitation powers, as indicated by the symbols in Fig. 5 inset. The solid line is a fit to a model for light scattered by two-level systems[21]:

$$I_{PL} = \frac{I_0 P}{P_0 + P}. \quad (4)$$

Here, I_0 is the intensity limit approached at high input

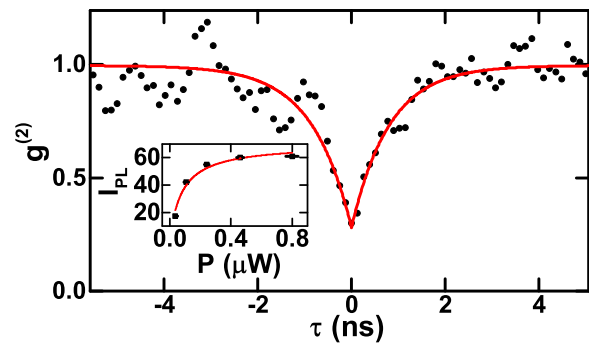


FIG. 5. Photon auto-correlation $g^{(2)}$ for center D_1 in Fig. 2(c). The excitation spot was offset from the detection spot to reduce the background emission. The contribution from the background has been corrected. Single-photon nature is confirmed by the observation of $g^{(2)}(0) < 0.5$. Inset: power dependence of emission intensity (symbols). The superimposed line is a fit to Eq. 4 yielding $P_0 = 77$ nW.

power and P_0 is the saturation input power, defined as the input power at which the intensity reaches $\frac{1}{2}I_0$. The saturation points to a finite number of two-level centers and also hinders the observation of bound excitons under high excitation power, as observed in Fig. 2(a).

In order to confirm the single-photon nature of the emission, we measured the second-order auto-correlation function $g^{(2)}(\tau)$ of the center D_1 of Fig. 2(c) using a Hanbury-Brown and Twiss setup. The $g^{(2)}$ histogram in Fig. 5 shows the characteristic dip at zero delay $\tau = 0$, signaling photon anti-bunching. The solid line is a fit to delay dependence of the form $g^{(2)}(\tau) = 1 - (1/N_p) \exp(-|\tau|/\tau_R)$. The fit yields an average number of simultaneously emitted photons at zero delay $N_p < 0.5$, thus confirming the single-photon nature of the emission. Finally, the fitted decay time constant $\tau_R = 0.8$ ns is comparable with the values measured for self-assembled InAs/GaAs QDs.[22]

In conclusion, we have reported the selective excitation of single excitons bound to shallow impurity centers via resonant tunneling in GaAs DQW structures. The observation of these centers becomes possible because of the blockade of carrier tunneling to form intrinsic exciton states over a range of applied electric fields. The latter hinders the formation of IXs, thus opening a gap in the emission spectrum. The PL within this gap is dominated by the dissociation of trions via tunneling process involving excitons bound to isolated shallow impurity centers. These bound excitons behave as two-level systems emitting single photons, as confirmed by the observation of anti-bunching in the photon autocorrelation histogram.

Single-photon emitters based on shallow centers profit from the well-developed semiconductor processing techniques. A major advantage of these centers is the much narrower distribution of emission energies as compared, for instance, to single-photon sources based on

self-assembled quantum dots. In contrast to previously reported impurity-based single-photon emitters on (Al,Ga)As structures,[23, 24] these bound excitons are electrically controlled and can be easily integrated with other functionalities such as site control and spin injection. The electrical control enables the isolation of individual centers by in-situ fabrication of electrostatic gates.[25] The shallow centers in GaAs DQWs are promising single photon emitters with both optical and electrical controls.

We thank S. Ludwig and M. Ramsteiner for many helpful discussions and suggestions. We thank S. Takada, C. Bäuerle, S. Rauwerdink, S. Meister and C. Hubert for support in sample fabrication. We acknowledge financial support from the German Forschungsgemeinschaft, DFG.

* yuan@pdi-berlin.de

- [1] H. R. Zeller and I. Giaever, *Phys. Rev.* **181**, 789 (1969).
- [2] M. A. Kastner, *Rev. Mod. Phys.* **64**, 849 (1992).
- [3] D. A. B. Miller, D. S. Chemla, T. C. Damen, A. C. Gosard, W. Wiegmann, T. H. Wood, and C. A. Burrus, *Phys. Rev. Lett.* **53**, 2173 (1984).
- [4] Y. J. Chen, E. S. Koteles, B. S. Elman, and C. A. Armiento, *Phys. Rev. B* **36**, 4562 (1987).
- [5] T. Huber, A. Zrenner, W. Wegscheider, and M. Bichler, *Phys. Status Solidi A* **166**, R5 (1998).
- [6] R. Rapaport, G. Chen, S. Simon, O. Mitrofanov, L. Pfeiffer, and P. M. Platzman, *Phys. Rev. B* **72**, 075428 (2005).
- [7] A. T. Hammack, N. A. Gippius, S. Yang, G. O. Andreev, L. V. Butov, M. Hanson, and A. C. Gossard, *J. Appl. Phys.* **99**, 066104 (2006).
- [8] G. J. Schinner, E. Schubert, M. P. Stallhofer, J. P. Kotthaus, D. Schuh, A. K. Rai, D. Reuter, A. D. Wieck, and A. O. Govorov, *Phys. Rev. B* **83**, 165308 (2011).
- [9] A. Violante, K. Cohen, S. Lazić, R. Hey, R. Rapaport, and P. V. Santos, *New J. Phys.* **16**, 033035 (2014).
- [10] G. J. Schinner, J. Repp, K. Kowalik-Seidl, E. Schubert, M. P. Stallhofer, A. K. Rai, D. Reuter, A. D. Wieck, A. O. Govorov, A. W. Holleitner, and J. P. Kotthaus, *Phys. Rev. B* **87**, 041303 (2013).
- [11] We use electric field instead of bias to take into account screening effects.
- [12] Y. Takahashi, Y. Kato, S. S. Kano, S. Fukatsu, Y. Shiraki, and R. Ito, *J. Appl. Phys.* **76**, 2299 (1994).
- [13] J. A. Brum, C. Priester, and G. Allan, *Phys. Rev. B* **32**, 2378 (1985).
- [14] Q. X. Zhao, T. Westgaard, B. O. Fimland, and K. Johannessen, *Phys. Rev. B* **45**, 11346 (1992).
- [15] M. Bayer and A. Forchel, *Phys. Rev. B* **65**, 041308 (2002).
- [16] L. W. Molenkamp, R. Eppenga, G. W. 't Hooft, P. Dawson, C. T. Foxon, and K. J. Moore, *Phys. Rev. B* **38**, 4314 (1988).
- [17] M. J. Snelling, E. Blackwood, C. J. McDonagh, R. T. Harley, and C. T. B. Foxon, *Phys. Rev. B* **45**, R3922 (1992).
- [18] K. J. Nash, M. S. Skolnick, P. A. Claxton, and J. S. Roberts, *Phys. Rev. B* **39**, 10943 (1989).
- [19] S. N. Walck and T. L. Reinecke, *Phys. Rev. B* **57**, 9088 (1998).
- [20] G. Brozak, B. D. McCombe, and D. M. Larsen, *Phys. Rev. B* **40**, 1265 (1989).
- [21] B. R. Mollow, *Phys. Rev.* **188**, 1969 (1969).
- [22] V. Zwiller, H. Blom, P. Jonsson, N. Panev, S. Jeppesen, T. Tsegaye, E. Goobar, M.-E. Pistol, L. Samuelson, and B. Björk, *Appl. Phys. Lett.* **78**, 4276 (2001).
- [23] S. Minari, L. Cavigli, F. Sarti, M. Abbarchi, N. Accanto, G. M. Matutano, S. Bietti, S. Sanguinetti, A. Vinattieri, and M. Gurioli, *Appl. Phys. Lett.* **101**, 172105 (2012).
- [24] M. Ikezawa, Y. Sakuma, L. Zhang, Y. Sone, T. Mori, T. Hamano, M. Watanabe, K. Sakoda, and Y. Masumoto, *Appl. Phys. Lett.* **100**, 042106 (2012).
- [25] M. Gschrey, F. Gericke, A. Schler, R. Schmidt, J.-H. Schulze, T. Heindel, S. Rodt, A. Strittmatter, and S. Reitzenstein, *Appl. Phys. Lett.* **102**, 251113 (2013).

**SUPPLEMENTARY MATERIAL FOR:
TUNNELING BLOCKADE AND SINGLE-PHOTON EMISSION IN GAAS DOUBLE QUANTUM WELL
STRUCTURES**

SPECTROSCOPIC EXPERIMENTS

The microscopic photoluminescence (μ -PL) experiments were carried out in a helium bath cryostat at 4.2 K (Attocube Confocal Microscope) with positioning control provided by a piezoelectric stage. The incoming laser with a wavelength of 780 nm was focused on the sample surface using an objective with numerical aperture of $NA \sim 0.8$. The laser energy lies below the band-gap of the $Al_{0.3}Ga_{0.7}As$ barriers and thus selectively excites electron hole pairs only in the GaAs QWs. The diameter of the laser spot $\phi_L = 1.2 \mu m$ sets the spatial resolution to $0.6 \mu m$. The PL was collected by the same objective and coupled to a monochromator using either a single-mode optical fiber (for confocal measurements) or by a fiber bundle (for spatially resolved measurements). The input slit of the monochromator was selected to yield a spectral resolution of 0.08 meV. A liquid-nitrogen cooled CCD detector was used to detect the light at the output port of the monochromator. The dimensions of each CCD pixel corresponds to $0.35 \mu m$ on the sample.

The photon auto-correlation studies were carried out using a Hanbury-Brown and Twiss setup. The PL from the shallow center was collected by the objective, filtered by a Semrock band-pass filter with a bandwidth of 810 ± 1.5 nm and then coupled to a single-mode fiber connected to a 50/50 fiber splitter. The outputs of the fiber splitters were then sent to a pair of superconducting single-photon detectors (Single Quantum Eos). The coincidence statistics was performed by a PicoQuant Picoharp photon counting system with a time bin of 128 ps.

**BLOCKADE FEATURE UNDER VARYING
POWER AND TEMPERATURE**

Spatially integrated PL vs. bias voltage V_b maps were measured at 4.2 K for different laser excitation powers. A few examples are shown in Fig. SM1. At high excitation power the blockade is no longer visible anymore. The blockade energy ΔE_B is extracted as the energy difference between T and the onset energy of the IX detected when the bias is tuned beyond the flat-band range. We plot ΔE_B for the lowest four excitation power P in Fig. SM2 and find that the blockade stays between Δ_1 and Δ_2 defined by Eqs. 1 and 2 of the main text.

As expected, rising temperature smears out the blockade feature, making it harder to identify, as shown in Fig. SM3.

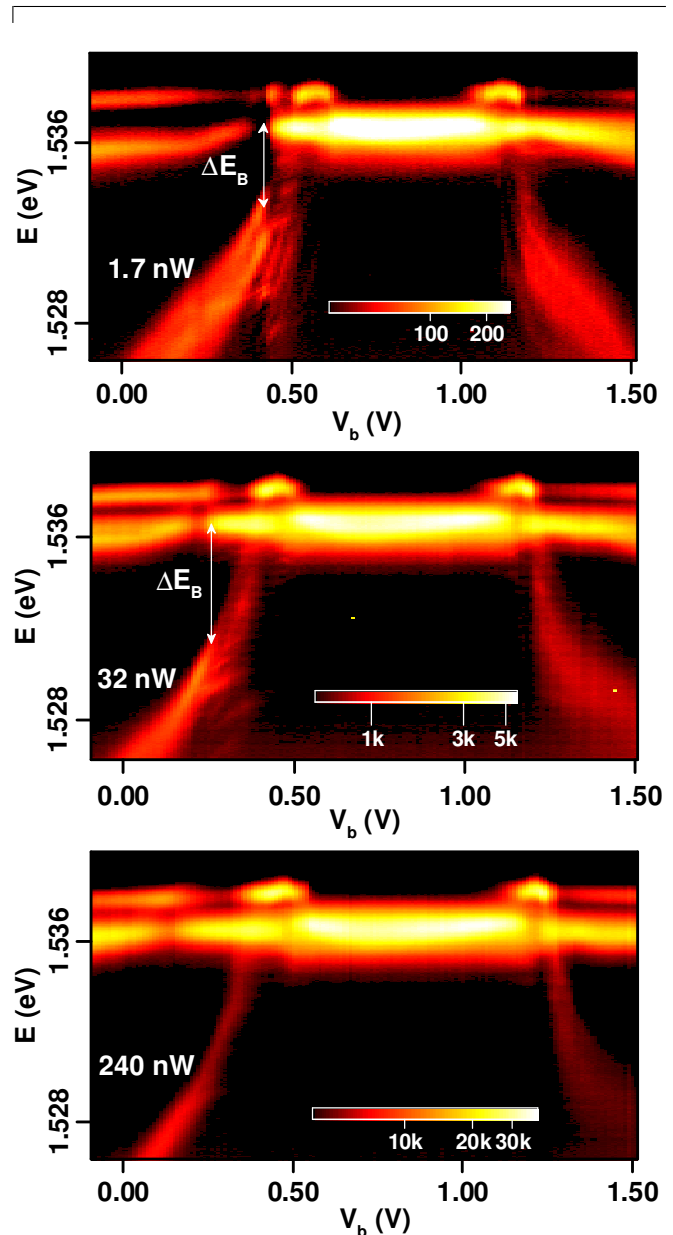


FIG. SM1. Spatially integrated PL as a function of bias voltage V_b recorded under different optical excitation power

ACTIVATION ENERGY

By varying the sample temperature T we thermally quench the PL intensity for another bound exciton, D_3 at 1.529 eV, from which we extract the activation energy E_A for its dissociation. The probability of thermal activation obeys the Boltzmann's law

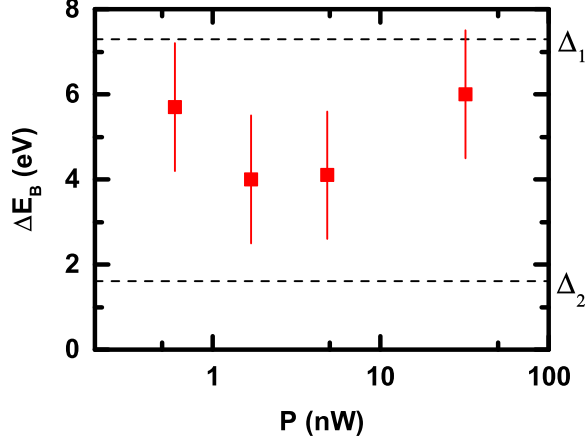


FIG. SM2. Blockade range ΔE_B extracted at different laser power P .

$$p \propto \exp \left[-\frac{E_A}{k_B T} \right]. \quad (\text{SM1})$$

Here, k_B is the Boltzmann constant. The PL quantum efficiency can be expressed as

$$\eta = \frac{1}{1 + \xi \exp(-E_A/k_B T)}, \quad (\text{SM2})$$

where ξ is a constant. The intensity of PL is proportional to its quantum efficiency, and thus decreases with rising temperature, as can be seen in Fig. SM4(a).

We can express the inverse of the PL intensity, letting $\alpha = 1/T$, as

$$\frac{1}{I_{PL}} = A + B \exp \left(-\frac{E_A}{k_B} \alpha \right), \quad (\text{SM3})$$

where A and B are additional constants. By fitting the data with Eq. SM3 (see Fig. SM4(b)), we extract $E_A = 6.5$ meV, which is comparable with the energy difference between trion T and the defect center D₃, 7 meV.

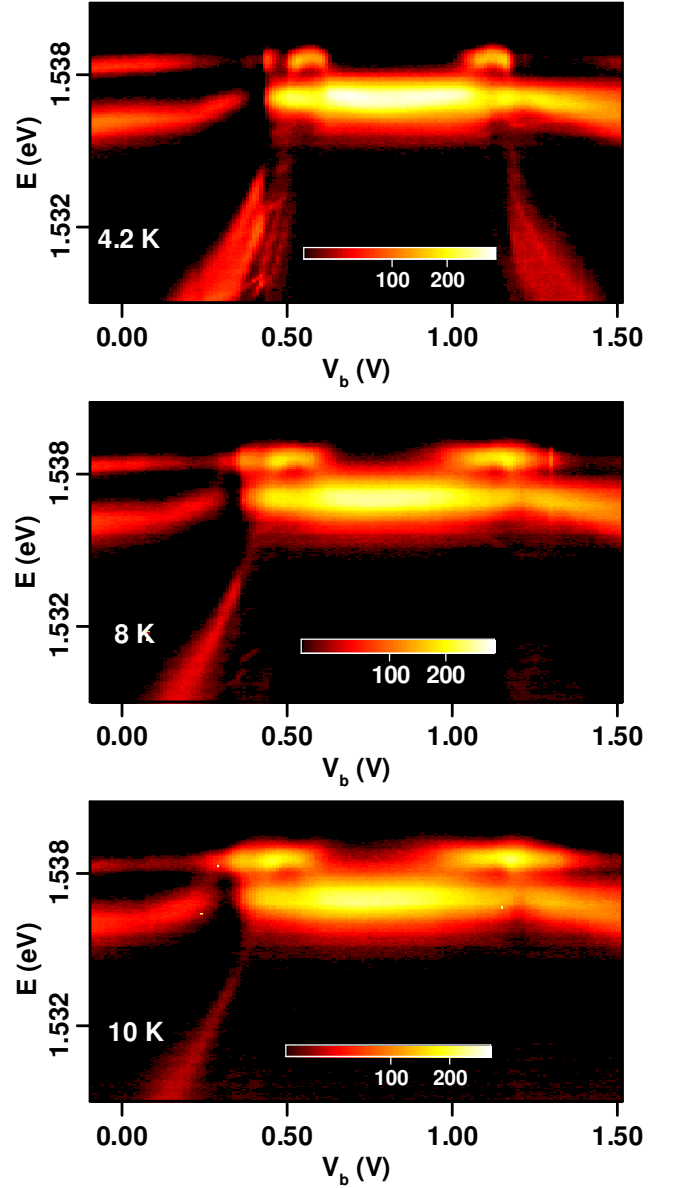


FIG. SM3. Spatially integrated PL as a function of bias voltage V_b recorded under different temperature. Laser power is kept at 1.7 nW.

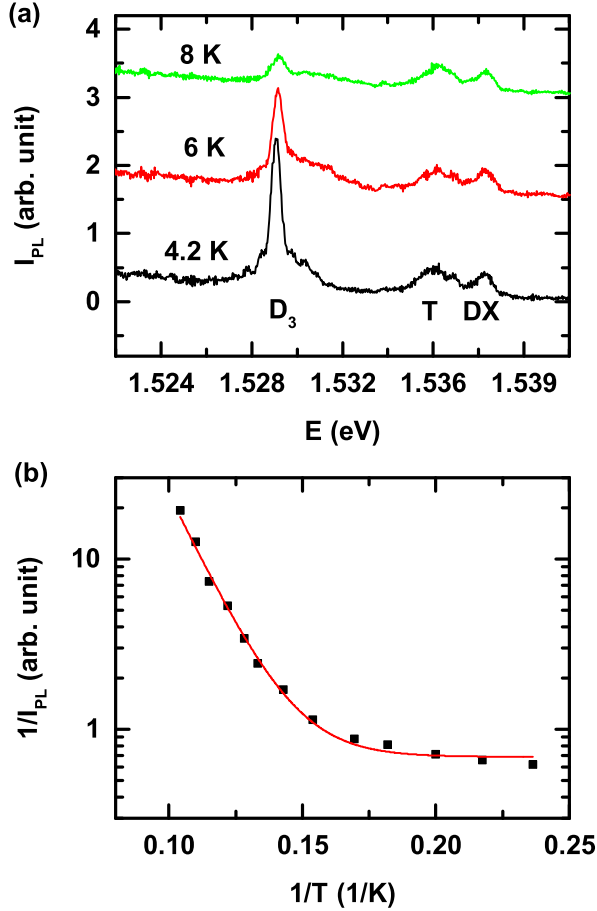


FIG. SM4. (a) Spectrum taken at different temperature, showing the thermal quenching of I_{PL} from D_3 at 1.529 eV. (b) The inverse of PL in logarithmic scale vs. the inverse of temperature. Solid: data. Line: fit.

LIST OF ABBREVIATIONS AND SYMBOLS

QW	quantum well
DQW	double quantum well
DX	direct exciton
T	trion
IX	indirect exciton
CB	conduction band
VB	valence band
QCSE	quantum-confined stark effect
MBE	molecular beam epitaxy
PL	photoluminescence
μ -PL	microscopic photoluminescence
SM	supplementary material
FB	flat-band
BR	blockade regime
DX^b	bound exciton with DX-like bias-dependence
IX^b	bound exciton with IX-like bias-dependence
$D_{1,2,3}$	individual bound excitons
F_z	transverse electric field
V_b	bias voltage
d_{QW}	QW thickness
d_b	barrier thickness
ϕ_c	Ti contact diameter
I_{PL}	PL intensity
ϕ_L	laser spot diameter
λ	laser wavelength
P	laser power
ΔE_B	energy gap between onset of IX and T
E_{IX}	IX energy
E_T	T energy
E_{DX}	DX energy
E_g	bandgap energy
ΔE_{IX}	IX binding energy relative to bandgap
ΔE_{T-DX}	T binding energy relative to DX
ΔE_{DX}	DX binding energy relative to bandgap
Δ_1	energy difference between T and bandgap
Δ_2	energy difference between T and DX
n_d	areal density of shallow impurities
Γ_S	spectral linewidth in frequency
ΔE_A	activation energy
$\Delta E^{(d)}$	diamagnetic energy shift
$\Delta E^{(z)}$	Zeeman splitting
e	electron charge
μ	reduced excitonic mass
m_e	electron mass
m_{hh}	heavy hole mass
ρ	extent of exciton wave function
B_z	transverse magnetic field
g	Landé g-factor
μ_B	Bohr magneton
$g^{(2)}$	second-order auto-correlation function
τ	time delay
N_p	number of simultaneously emitted photons
τ_R	anti-bunching time constant
Γ_R	anti-bunching linewidth in frequency